IEEE Access
Multidisciplinary | Rapid Review | Open Access Journal

Received 6 July 2025, accepted 27 July 2025, date of publication 4 August 2025, date of current version 13 August 2025.

Digital Object Identifier 10.1109/ACCESS.2025.3595193

RESEARCH ARTICLE

Demonstration Platform to Emulate Cognitive GEO-LEO Dual Satellite System

KITHMINI WETHTHASINGHE[1], (Graduate Student Member, IEEE), YING HE[1], (Senior Member, IEEE), QUYNH TU NGO[1], (Senior Member, IEEE), BEESHANGA JAYAWICKRAMA[1], (Senior Member, IEEE), AND ERYK DUTKIEWICZ[2], (Senior Member, IEEE)

[1]School of Electrical and Data Engineering, University of Technology Sydney, Sydney, NSW 2007, Australia
[2]Faculty of Engineering and IT, University of Technology Sydney, Sydney, NSW 2007, Australia

Corresponding author: Kithmini Weththasinghe (Kithmini.WeththasingheArachchige@uts.edu.au)

This work was supported by the SmartSat CRC, whose activities are funded by the Australian Government's CRC Program.

ABSTRACT Cognitive radio technology represents a transformative advancement in modern telecommunications, enabling real-time adaptation and optimisation of communication systems through sensing, analysis, and decision-making. In the context of satellite communications, cognitive satellite networks leverage these capabilities to enable dynamic spectrum access, dynamic resource management, and adaptive network optimisation. These enhancements improve spectral efficiency, maximise bandwidth utilisation, and enhance overall network performance, leading to more scalable, resilient, and cost-effective satellite operations. In this study, we develop a laboratory-scale demonstration platform to emulate a cognitive GEO-LEO dual satellite system using software-defined radios, which operate under controlled conditions without incorporating orbital dynamics such as Doppler effects or variable angular velocities. The geostationary satellite is designated as the primary user (PU), while the LEO satellite operates as the secondary user (SU). A preamble detection-based sensing algorithm is developed to identify PU transmissions, ensuring efficient spectrum utilisation. Additionally, a radio environment map (REM) server is implemented to manage control-plane data required for network decision-making. A dynamic spectrum access algorithm, integrated into the REM server, utilises spectrum sensing reports to enable cognitive network behaviour. We evaluate the performance of the PU and SU in terms of spectral occupancy and throughput. Furthermore, the performance of the proposed sensing algorithm is assessed based on missed detection rates. The results demonstrate that the cognitive system's dynamic spectrum access capabilities significantly enhance spectral occupancy and system throughput, validating its effectiveness in optimising satellite communication networks.

INDEX TERMS Cognitive satellite radio, demonstration platform, dynamic spectrum access, radio environment map, spectrum sensing.

I. INTRODUCTION

In the constantly evolving landscape of wireless communications, cognitive radio (CR) technology has emerged as a paradigm-shifting approach for efficiently utilising the increasingly congested radio frequency spectrum [1], [2], [3], [4]. In contrast to traditional static spectrum allocation, CR systems leverage adaptive intelligence to dynamically perform spectrum allocation based on real-time environmental conditions. This enables efficient spectrum utilisation while mitigating interference to incumbent users through real-time spectrum sensing and decision-making processes. The dynamic and adaptive nature of CR systems holds great promise for enhancing the efficiency and reliability of wireless communication networks, making them more resilient and capable of meeting the growing demand for wireless services.

In the context of satellite communications, this technology manifests as cognitive satellite radio (CogSat), which enhances the efficient allocation and management of

The associate editor coordinating the review of this manuscript and approving it for publication was Faissal El Bouanani.

temporal, spectral, and spatial resources in satellite communication systems [5]. The primary objective of CogSat is to elevate system performance, particularly in environments with unpredictable traffic conditions, including primary and secondary user transmissions, incidental interference, and deliberate jamming. Cognitive satellite networks enhance satellite communications by enabling dynamic spectrum sharing, optimising resource allocation, and increasing network capacity, resulting in more efficient and cost-effective operations.

In contrast to geostationary (GEO) satellites, low Earth orbit (LEO) systems significantly reduce signal latency due to their proximity to Earth, making them ideal for latency-critical applications such as broadband communications, real-time data streaming, and high-frequency trading [6], where rapid data transmission is essential. This enhanced significance of LEO satellites drives a surge in their deployment within the evolving satellite ecosystem. However, their limited footprint necessitates large-scale constellations for seamless global coverage. Consequently, the satellite architecture is transitioning into a multi-tier framework, where LEO networks enhance low-latency performance, while GEO satellites remain integral for continuous, wide-area coverage in applications like broadcasting, meteorology, and aviation communications.

The growing density of satellites in orbit has intensified spectrum congestion in frequency bands, particularly sub-GHz ranges. However, extensive occupation by incumbent users limits the frequency availability. CR technology offers a solution to these challenges by enabling satellite systems to intelligently share spectrum resources [7]. CR systems can sense the spectrum environment, identifying unused or underutilised spectrum bands. This allows satellite systems to opportunistically access these idle bands for data transmission without causing interference to primary users [8].

Spectrum-sharing techniques offer distinct approaches for secondary users, also known as cognitive users, to operate alongside primary users, also referred to as incumbents, while optimising spectrum utilisation and minimising interference [9], [10]. In cognitive networks, when incumbent users are not actively utilising the spectrum, secondary users are allowed to transmit using the spectrum interweave technique. These techniques implement dynamic access strategies, interference mitigation protocols, and adaptive resource allocation to ensure seamless coexistence within shared frequency bands.

Spectrum sensing and analysis techniques are employed to identify available frequencies, enabling secondary users to utilise them effectively and to detect the reactivation of licensed spectrum usage by primary users, thereby preventing any potential interference. Utilising spectrum management and seamless handoff capabilities, secondary users can intelligently select the most suitable frequency bands and ensure a smooth transition between multiple bands, adapting to changing channel conditions. In order to achieve optimal spectrum efficiency in the context of dynamic spectrum access, it is crucial to establish efficient systems for spectrum allocation and sharing. This enables effective collaboration among secondary users, primary users, and other secondary users in making the most of shared resources [11], [12], [13], [14]. Among the spectrum sensing techniques utilised in cognitive radio systems, the energy detection method stands out as the simplest, as it solely requires the measurement of received signal energy.

Many real-time implementations of CR systems in the literature leverage software-defined radio (SDR) platforms. SDR is a fundamental component of communication systems, replacing dedicated hardware for certain functions with software that runs on embedded systems or computers. SDR technology offers efficient resource utilisation and management within communication systems. In contrast to traditional hardware-based communication systems, where system modifications require physical alterations, incurring significant costs, SDR allows for easy and cost-effective upgrades through software modifications [15]. Consequently, this approach can enhance the transmission quality of the system. Popular SDR tools include GNU Radio and universal software radio peripheral (USRP) hardware [16]. GNU Radio, an open-source software tool, incorporates firmware for USRP devices and is programmable using both C++ and Python. It offers a wide array of libraries for digital signal processing. In terms of hardware components, the USRP device serves as a versatile platform that can function as both a transmitter and a receiver. Its real-time data transmission capabilities can adapt to various characteristics, depending on the technical specifications of the hardware. Notably, USRP can be programmed using GNU Radio, offering flexibility in implementation choices.

The study in [17] implemented a fully operational communication system for interference detection, utilising USRPs as the SDR platform. In [18], a real-time, adaptive threshold energy detector was designed and validated using a USRP-based SDR system. The study in [19] designed a testbed for distributed decision fusion in virtual massive multiple-input multiple-output systems, facilitating collaborative wideband spectrum sensing within a cognitive radio-like network. Additionally, [20] proposed a model for energy detection-based spectrum sensing. The study in [17] implemented a fully functional communication system for interference detection, leveraging USRPs as the SDR platform. Paper [18] built and tested a real-time, adaptive threshold energy detector using a USRP SDR. Paper [19], developed a testbed for virtual massive multiple-input-multiple output-based distributed decision fusion for collaborative wideband spectrum sensing in a cognitive radio-like network. Reference [20], developed a model to perform an Energy Detection-Based Spectrum sensing. In [10], a system was designed to acquire downlink signals from a GEO satellite. This implementation utilised a standalone spectrum sensing node, leveraging an SDR USRPB200

for signal acquisition. Subsequently, [21] introduced a cooperative spectrum sensing framework wherein multiple USRP B200 devices, each equipped with a GPS-disciplined oscillator (GPSDO), were employed. The GPSDO-enabled synchronisation mechanism facilitated precise GPS-based time alignment between USRP units, ensuring temporal coherence between independently captured signal datasets.

This study illustrates the coexistence of a GEO satellite as the primary user (PU) and a LEO satellite as the secondary user (SU), functioning within a cognitive system. The LEO satellite opportunistically accesses unused GEO spectrum based on the outcome of spectrum sensing. We highlight sensing capabilities on the sensors and channel allocation capabilities on the radio environment map (REM) server, demonstrating the cognitive functionalities of the system.

The main contributions of this study are summarised below.

1) Develop a laboratory-scale demonstration platform that serves as a proof-of-concept system, to emulate the cognitive GEO-LEO satellite system using SDRs, considering the GEO satellite as PU and the LEO satellite as SU.
2) Develop a preamble detection-based sensing algorithm to identify the presence of PU transmissions and synchronisation.
3) Design and implement a REM server to manage control plane data, facilitate communication with network nodes and handle spectrum-related control signals, including access requests, grants, and sensing reports.
4) Develop a dynamic spectrum allocation algorithm at the REM server, leveraging spectrum sensing reports to identify available channels for SU transmission while preventing interference with PUs.
5) Implement a scheduler at the SU transmission node to enable dynamic channel allocation to multiple SU receivers based on predefined criteria, ensuring optimised spectrum utilisation and cognitive network behaviour.

The rest of the paper is organised as follows. Section II describes the considered system model. Section III provides a detailed description of the data plane design of primary and secondary systems. Section IV explains the proposed REM architecture and control plane design. Section V is about the performance metrics employed in the system performance evaluation. Section VI presents the measurement results and discussion. Section VII includes possible future work. Finally, section VIII concludes the paper.

II. SYSTEM MODEL

We model a cognitive dual satellite system in which a multibeam GEO satellite functions as the primary user (PU), while a LEO satellite operates as the secondary user (SU). The GEO satellite employs a multi-beam transmission architecture using directional antennas, with each beam operating on a distinct frequency band to mitigate inter-beam interference. Specifically, we model a GEO system with two independent spot beams, each serving a different ground user on separate frequencies. Given the larger footprint of the LEO satellite compared to a single GEO spot beam, we assume that the LEO satellite footprint encompasses both GEO spot beams, allowing it to access the spectrum associated with both frequencies. The LEO satellite, characterised by its compact design and omnidirectional antenna, enables both transmission and reception across its entire coverage footprint, as illustrated in Fig. 1.

This setup is designed for downlink communication, where GEO and LEO downlink transmissions coexist within the same frequency spectrum. Under these conditions, the cognitive LEO satellite must adapt its downlink transmissions to mitigate interference on GEO users. This necessitates dynamic spectrum sensing and resource allocation techniques to optimise frequency utilisation while minimising interference to the GEO satellite's primary transmissions. Two ground-based sensors within each GEO spot beam detect primary user activity and report their observations to a centralised Radio Environment Map (REM). Two LEO users are modelled on the ground, one with access to both frequency bands and another with access to only one, demonstrating heterogeneous CR capabilities and enabling performance evaluation in terms of throughput and spectrum utilisation. Upon receiving a spectrum request from the LEO satellite, the REM assigns an available channel, which the LEO satellite then allocates to one of its users based on a local scheduler. To emulate realistic operational conditions, we adopt a slot-based transmission structure where each slot is either fully occupied or idle, aligning with scheduled data transmission patterns seen in actual satellite communication systems. Preamble detection is employed to identify primary user activity, as energy detection alone is inadequate when the timing of transmissions is unknown. This experimental platform, while simplified, captures key characteristics of real-world GEO-LEO coexistence scenarios and provides a practical foundation for validating cognitive radio mechanisms in satellite networks.

In this context, we emulate the cognitive GEO-LEO dual satellite system using USRP SDRs as depicted in Fig. 2. The setup features a PU transmitter (PU TX) equipped with two antennas, simulating GEO traffic across two distinct frequency channels to model the spectral activity of two GEO beams. Two single-antenna PU receivers (PU RX1 and PU RX2) function as GEO users, each operating on a separate channel to receive the transmitted GEO data. In a cognitive GEO-LEO dual-satellite system, efficient and interference-free spectrum sharing is critical due to the overlapping coverage areas and the scarcity of available spectrum. A REM server plays a central role in enabling dynamic spectrum access by maintaining a real-time, global view of spectrum occupancy. This allows the system to intelligently coordinate transmissions, ensuring that the LEO satellite can access available spectrum without disrupting the GEO satellite's operations. To support this functionality,

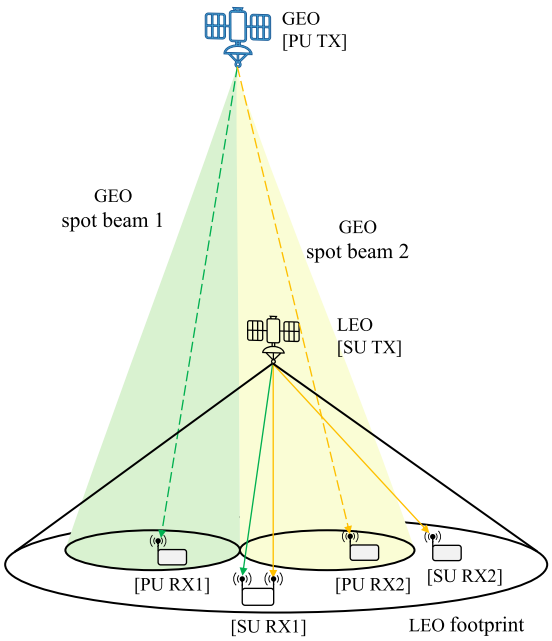

FIGURE 1. Cognitive GEO-LEO dual satellite model considered for demonstration platform.

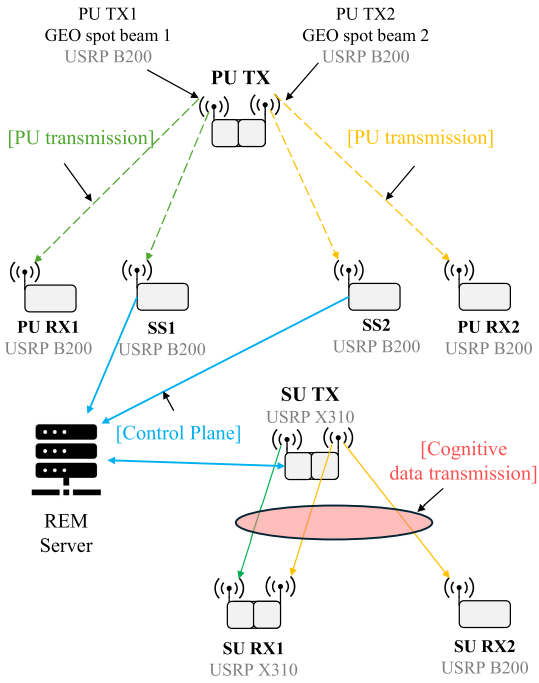

FIGURE 2. System architecture with SDRs, signalling, and control channels.

two single-antenna spectrum sensing nodes (SS1 and SS2) are deployed to monitor PU activity on their respective channels in real time. These sensing nodes report their observations to the REM server, which processes the data to identify spectrum holes and assess interference levels. Using a dynamic spectrum allocation algorithm, the REM server then determines the optimal transmission timing and frequency allocations for secondary users. This approach maximises spectral efficiency while preserving the quality of service for both primary and secondary users through adaptive, interference-aware coordination.

The LEO SU system consists of a two-antenna SU transmitter (SU TX), a two-antenna SU receiver (SU RX1), and a single-antenna SU receiver (SU RX2). This system dynamically accesses the two GEO channels based on availability, as determined by feedback from the REM server. The transmission of sensing reports and resource allocation information is managed via the control plane (CP) using a dedicated communication channel. The SU TX scheduler manages transmission initiation, termination, and seamless frequency band switching, enabling the secondary network to maintain a stable data stream by dynamically adjusting transmission parameters within the cognitive channel.

III. DATA PLANE OF PRIMARY AND SECONDARY SYSTEMS

The physical experimental setup of the demonstration platform is shown in Fig. 3. In this section, we present a comprehensive analysis of PU and SU transmitter and receiver architectures, including block diagrams and signal processing workflows. Furthermore, we discuss the design and operation of sensing nodes, including the sensing algorithm. Finally, we describe the proposed control plane and REM server architecture in detail.

A. PU TRANSMITTER

1) SLOT STRUCTURE

We model the PU's transmission using a slot-based structure, wherein each time slot, the PU either operates in an active state by transmitting continuously for the entire duration or remains idle for the full slot. This results in distinct transmission states, leading to well-defined intervals of active and idle transmissions, as illustrated in Fig. 4. The PU transmission slot structure consists of a preamble followed by data, where the preamble is represented by a Zadoff-Chu (ZC) sequence to enable robust signal identification [22]. The preamble x_P and data x_D lengths are denoted as L_P and L_D, respectively. This framework enables sensor nodes to detect PU activity by identifying the preamble, allowing for accurate classification of occupied and unoccupied time slots.

The ZC sequence is used as a preamble at the PU and SU transmitters. The q-th ZC sequence $s_q[n]$ is defined as

$$s_q[n] = exp\left[-j\pi q\frac{n(n+1)}{L}\right] \tag{1}$$

where $q = 0, \ldots, L-1$ is the root index and L is length of the ZC sequence with $L < L_P$. Subsequently, zero padding is applied to the ZC sequence to construct the preamble as in (2), ensuring spectral shaping and synchronisation efficiency. The root indices assigned to the PU for each PU channel are

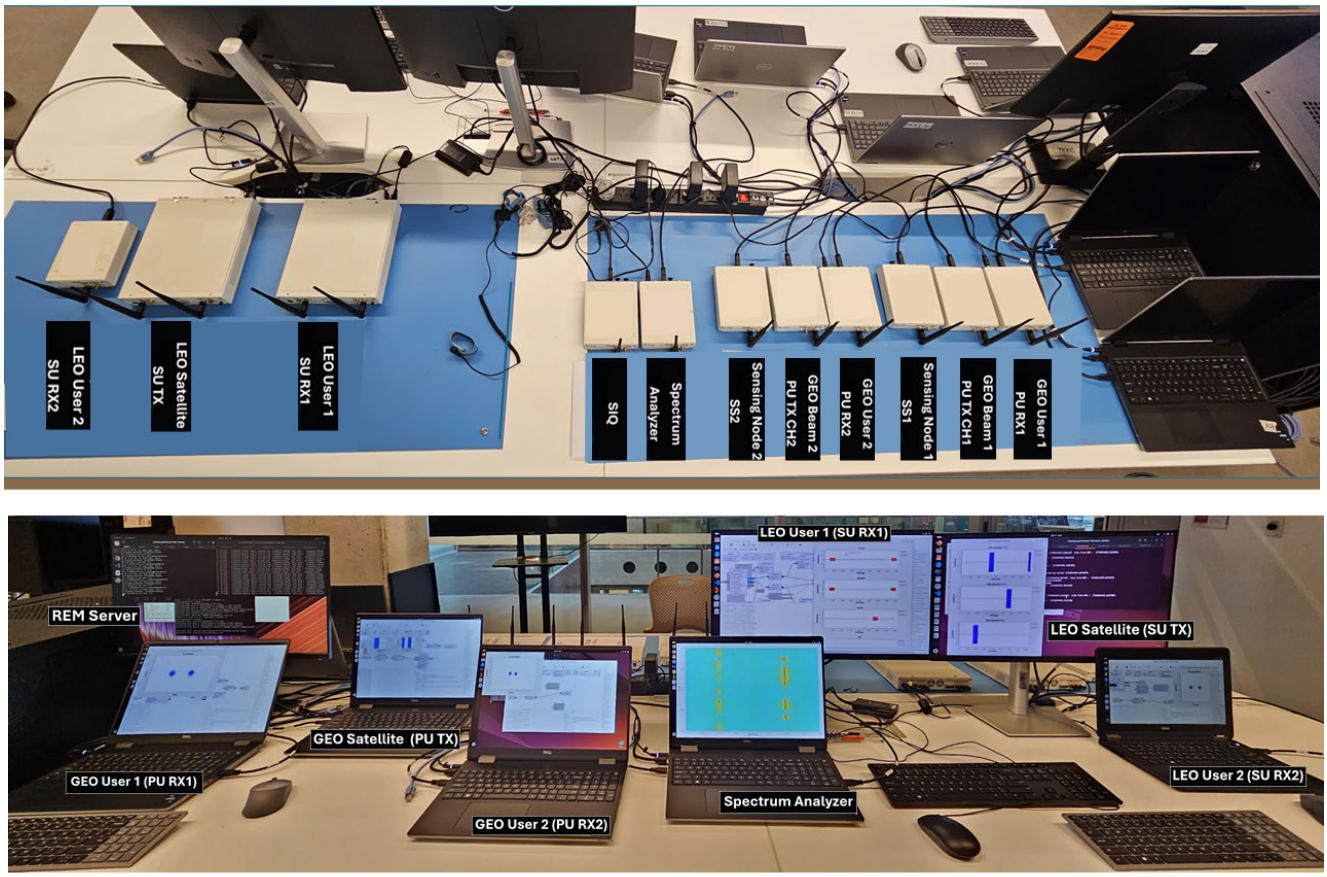

FIGURE 3. The proposed demonstration platform to emulate cognitive GEO-LEO dual satellite system.

denoted as $q_{p,1}$ and $q_{p,2}$.

$$x_P[n] = \begin{cases} 0, & n \in [-L_{pre}, -1] \\ s_q[n], & n \in [0, L-1] \\ 0, & n \in [L, L + L_{post} - 1] \end{cases} \quad (2)$$

where L_{pre} and L_{post} are the number of zeros padded before and after the sequence respectively.

2) PU TX ARCHITECTURE

The block diagram of the PU TX is depicted in Fig. 5a. Each RF channel within the PU TX is implemented using a USRP B200 SDR platform, which functions as the RF front end for signal transmission. The signal generation process is implemented on a host PC utilising the GNU Radio framework. In this setup, the PU TX transmits two distinct text files to PU RXs across two separate frequency channels, CH1 and CH2. The detailed architecture of the signal generation module is illustrated in Fig. 5b, outlining the key components and signal processing flow. Binary phase shift keying (BPSK) is utilised for data modulation.

B. PU RECEIVER

The PU receivers, PU RX1 and PU RX2, are identical single-antenna receiver architectures. During operation,

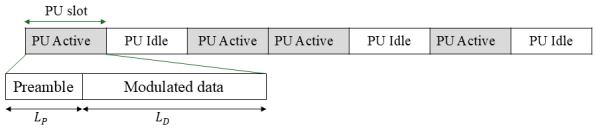

FIGURE 4. A random PU transmission pattern.

PU RX1 is configured to receive signals on CH1, while PU RX2 is tuned to CH2. Each PU receiver's RF front end is implemented using the USRP B200 SDR platform, enabling flexible frequency tuning and signal reception. The detailed block diagram of the PU receiver architecture is presented in Fig. 6a.

The architecture of the PU RX is depicted in Fig. 6b. Incoming signals first pass through a preamble detection module, which extracts the preamble and facilitates the decoding of the received BPSK-modulated signal. The detected BPSK signal is then processed by an automatic gain control (AGC) block, which normalises its amplitude to ensure consistent signal levels. Next, the signal undergoes coarse frequency correction via a frequency-locked loop (FLL) band-edge filter. Following this, a symbol synchronisation module aligns the signal with symbol timing to accurately recover the transmitted data. A Costas

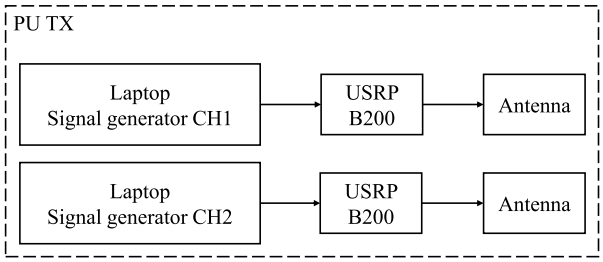

(a) PU TX block diagram.

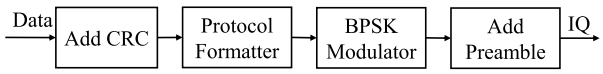

(b) PU TX signal generator block diagram.

FIGURE 5. PU TX block diagram and transmission signal generating process.

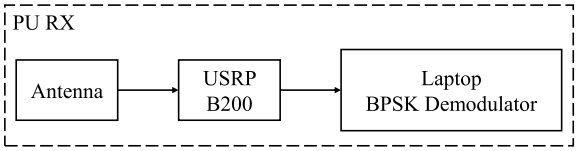

(a) PU RX block diagram.

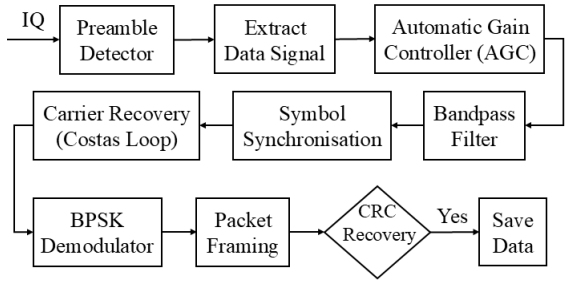

(b) Implementation of PU RX.

FIGURE 6. PU RX block diagram and data decoding process.

loop is then employed for fine carrier phase recovery, ensuring precise demodulation of the BPSK constellation. The demodulated symbols are subsequently processed by a constellation decoder, followed by a differential decoder to resolve any phase ambiguities. To establish proper framing, the bitstream is correlated with a predefined access code and tagged for data frame alignment. The recovered bits are restructured into the required format and subjected to integrity verification using a cyclic redundancy check (CRC). Finally, the processed data stream is written to an output file, marking the completion of the demodulation process.

C. SENSOR NODE

1) SENSOR NODE ARCHITECTURE

The sensor nodes, SS1 and SS2, are identical single-antenna devices as depicted in Fig. 7a. During operation, SS1 and SS2

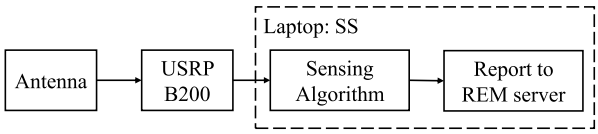

(a) Spectrum sensors: SS1 and SS2 block diagram.

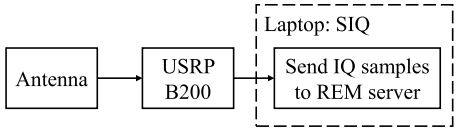

(b) IQ sensor: SIQ block diagram.

FIGURE 7. Sensor nodes block diagrams.

are tuned to CH1 and CH2, respectively, to sense PU activity using a preamble detection-based sensing algorithm. The RF channel for each sensor node is implemented using the USRP B200 platform. Upon successful preamble detection. the sensor sends the sensing report to the REM server. Due to the binary nature of the PU slot state, sensing nodes classify the entire slot as busy if PU activity is detected during the sensing period; otherwise, it is designated as free. In scenarios where the receiver fails to detect a preamble, the resulting missed detection impacts the channel status solely within the duration of a single slot.

IQ sensor (SIQ) is a single-antenna device, as illustrated in Fig. 7b, designed to capture in-phase (I) and quadrature (Q) samples for the REM visualisation platform.

2) PREAMBLE DETECTION

Preamble detection is performed by identifying a predefined ZC sequence within the received signal [23]. This is achieved through cross-correlation between the received signal y with the expected preamble x_P, which is generated using a ZC sequence with designated root index q, as specified by (1) and (2) [24]. The proposed FFT-based cross-correlation method is formulated below.

$$\mathcal{R}_{x,y} = \left(\mathcal{F}^{-1}\left\{X(f)\cdot Y^{*}(f)\right\}\right)^{2}/N_{fft} \tag{3}$$

where $X(f) = \mathcal{F}\{x[n]\}$ and $Y(f) = \mathcal{F}\{y[n]\}$. $Y^{*}(f)$ is the complex conjugate of $Y(f)$ and $\mathcal{F}^{-1}$ denotes the inverse FFT (IFFT). The receiver analyses the correlation values to determine the preamble's position, where the highest correlation peak, $\mathcal{R}^{max}_{x,y}$, signifies its starting point. The ratio between the peak and average values of the correlation results is calculated as $\mathcal{R}^{max}_{x,y}/\mathcal{R}^{avg}_{x,y}$. Detection is confirmed if the ratio exceeds a predefined threshold Γ, enabling precise frame synchronisation and facilitating subsequent data decoding. The proposed preamble detection algorithm is summarised in Algorithm 1.

D. SU TRANSMITTER

The SU TX block diagram, shown in Fig. 8a, includes two antennas implemented with a USRP X310 featuring two RF

Algorithm 1 Preamble Detection Algorithm

Input: y // Signal received at the receiver
Constants: L, L_P, q, Γ
Initialise: $\mathcal{R}_{x,y}^{max} \leftarrow 0$
$t_{id} \leftarrow -1$ // Detected preamble start index t_{id}
Generate ZC sequence s_q based on q using (1)
Construct preamble x_q using (2)
Preamble Detection:
Compute cross correlation $\mathcal{R}_{x,y}$ based on (3)
Get the maximum value $\mathcal{R}_{x,y}^{max} = max(\mathcal{R}_{x,y})$
Get the average value $\mathcal{R}_{x,y}^{avg} = average(\mathcal{R}_{x,y})$
Check Detection:
if $\mathcal{R}_{x,y}^{max} / \mathcal{R}_{x,y}^{avg} > \Gamma$ **then**
return t_{id} // Preamble detected at index t_{id}
else
return -1 // No preamble detected
end if

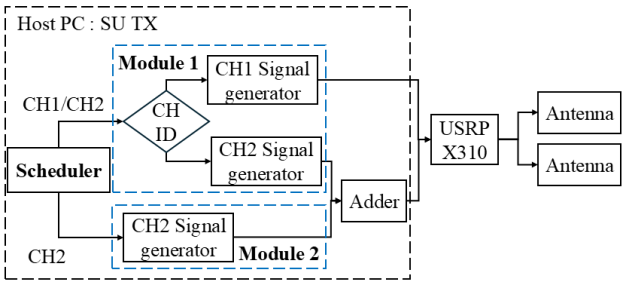

(a) SU TX block diagram.

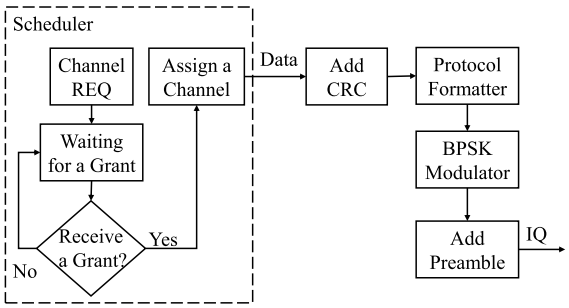

(b) SU TX signal generator block diagram.

FIGURE 8. SU TX block diagram and functional diagram.

modules. The operational flow of the SU TX is depicted in the flowchart in Fig. 8b. The SU TX sends a request (REQ) to the REM server for channel access. Upon receiving a grant specifying available channels and allowed transmission duration, the SU TX begins transmission. If no grant is received, the SU TX remains in a waiting state until access is granted. The SU utilises root indices $q_{s,1}$ and $q_{s,2}$ for SU RX1 and SU RX2, respectively.

The scheduler in SU TX manages channel allocation for SU receivers based on channel availability specified in the REM server's grant and channel requests from SU receivers. Algorithm 2 details the process for allocating channels to SU RX1 and SU RX2.

Algorithm 2 Secondary Multi-User Channel Allocation

Inputs: Requests for SU RX1 (R_1) and SU RX2 (R_2)
Outputs: Channel allocation for SU RX1 and/or SU RX2
Set $A_1 \leftarrow$ NULL, $A_2 \leftarrow$ NULL // Channel assignments for SU RX1 and SU RX2
if CH_1 and CH_2 are available **then**
  if $R_1 =$ TRUE and $R_2 =$ FALSE **then**
    // Assign both channels to SU RX1
    $A_1 \leftarrow A_1 \cup CH_1$
    $A_1 \leftarrow A_1 \cup CH_2$
  elseif $R_1 =$ FALSE and $R_2 =$ TRUE **then**
    $A_2 \leftarrow A_2 \cup CH_2$ // Assign CH_2 to SU RX2
  elseif $R_1 =$ TRUE and $R_2 =$ TRUE **then**
    $A_1 \leftarrow A_1 \cup CH_1$ // Assign CH_1 to SU RX1
    $A_2 \leftarrow A_2 \cup CH_2$ // Assign CH_2 to SU RX2
  end if
elseif only CH_1 is available **then**
  if $R_1 =$ TRUE **then**
    $A_1 \leftarrow A_1 \cup CH_1$ // Assign the channel to SU RX1
  else
    // No channel assignment
  end if
elseif only CH_2 is available **then**
  if $R_1 =$ TRUE and $R_2 =$ TRUE **then**
    // Assign the channel to the first requester
  else
    $A_1 \leftarrow A_1 \cup CH_2$ // Assign the channel to SU RX1
  end if
end if
return A_1, A_2 // Final channel allocations

E. SU RECEIVER

We define two types of SU receivers: SU RX1, which has access to both CH1 and CH2, and SU RX2, which is limited to access only CH2. SU RX1 is equipped with two antennas and implemented using a USRP X310 with two RF modules, allowing access to both channels, CH1 and CH2. The block diagram is shown in Fig. 9a. The signal processing flow, illustrated in Fig. 9b, involves receiving signals on both channels, performing preamble extraction via a detection block, and combining the BPSK signals from both channels before demodulation. SU RX2, implemented with a USRP B200 and a single antenna, has a similar implementation to PU RX, as described in section III-B. This configuration enables a clear evaluation of the dynamic spectrum sharing process.

IV. REM ARCHITECTURE AND CONTROL PLANE

The proposed REM architecture, illustrated in Fig. 10, incorporates a database for storing sensing data from SS1 and SS2. The dynamic spectrum allocation (DSA) algorithm, executed on the REM server, facilitates SU transmission. Performance metrics are collected from transmitters (PU TX, SU TX) and receivers (PU RX1, PU RX2, SU RX1, and SU

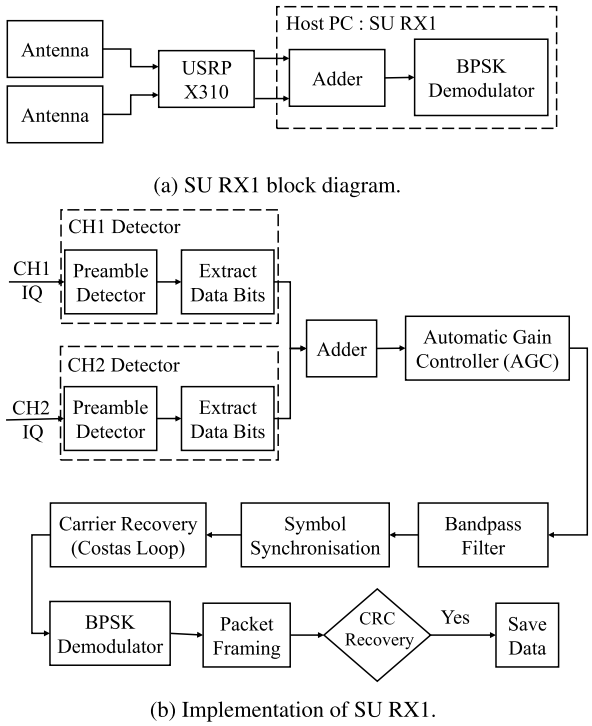

FIGURE 9. SU RX1 block diagram and data decoding process.

RX2) to evaluate the demonstration platform's performance. Spectrogram generation is achieved using FFT data obtained from the IQ sensor (SIQ).

To achieve network timing synchronisation, the precision time protocol (PTP) is used to synchronise clocks across the network with high accuracy. A PTP leader clock is set up at the REM server, acting as the central time source. It sends synchronisation messages to all connected nodes, including primary and secondary user transmitters and receivers, and sensor nodes. These nodes, configured as PTP follower clocks, adjust their local clocks to match the leader clock. The synchronisation process involves timestamped message exchanges to calculate delays and offsets, ensuring clock alignment with sub-microsecond accuracy for reliable time-sensitive tasks within the network.

The control plane connection for all nodes is managed through a central TL-SG1016 gigabit switch, ensuring seamless Ethernet connectivity. This switch acts as the backbone, facilitating efficient communication between nodes. The REM server, connected to the switch, oversees network management and synchronisation. The control plane handles essential data exchanges, including channel access, PTP synchronisation, configuration updates, and spectrum sensing results.

A. REM CONSTRUCTION PROTOCOL

The proposed REM construction protocol is illustrated in Fig. 11. We consider PU TX1 and PU TX2 operating on CH1 and CH2, respectively, with independent transmission

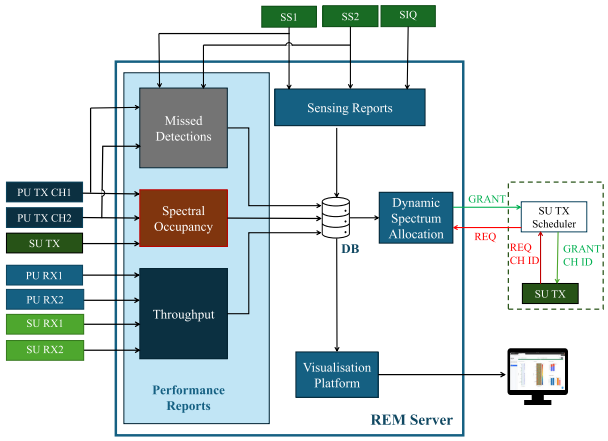

FIGURE 10. REM Server Architecture.

processes and slot durations. SS1 and SS2 perform spectrum sensing on CH1 and CH2, respectively. If SS1 detects PU activity on CH1 using Algorithm 1, it reports the detection to the REM server via the control plane. Similarly, SS2 reports PU activity on CH2. Notably, SS nodes do not monitor SU transmissions; they exclusively sense PU activity on the assigned channels.

When an SU TX has data to transmit, it initiates a transmission request (REQ) to the REM server. The REM server evaluates channel availability by executing Algorithm 3, utilising historical sensing reports and prior SU transmission records. If a given channel, CHi, is determined to be unoccupied, the REM server grants transmission permission to SU TX, specifying the available channel. Upon receiving the grant, SU TX initiates transmission in accordance with Algorithm 2 and REM server feedback. Upon completion of the allocated transmission slot, SU TX submits a subsequent REQ to the REM server if additional data remains for transmission. The key notations used in DSA algorithm are presented in Table 1.

B. DYNAMIC SPECTRUM ALLOCATION ALGORITHM

The proposed DSA algorithm is given in Algorithm 4. Consider current time is t and last sensing report received time is t_r, then expected PU transmission slot start time t_s and end time t_e are calculated as,

$$t_{diff} = t - t_r$$
$$t_s = t_r + \left(t_{diff} \bmod (d_{PU})\right) d_{PU} \quad (4a)$$
$$t_e = t_s + d_{PU} \quad (4b)$$

where t_{diff} is the time difference between current time t and the last sensing report time t_r. d_{PU} is the PU transmit duration.

The DSA algorithm enables the SU to access CH1 and CH2 without interfering with the PU transmission, as illustrated in Fig. 12. For instance, if the SU requests transmission at time t_1, the DSA algorithm defers the grant until t_2 due to ongoing

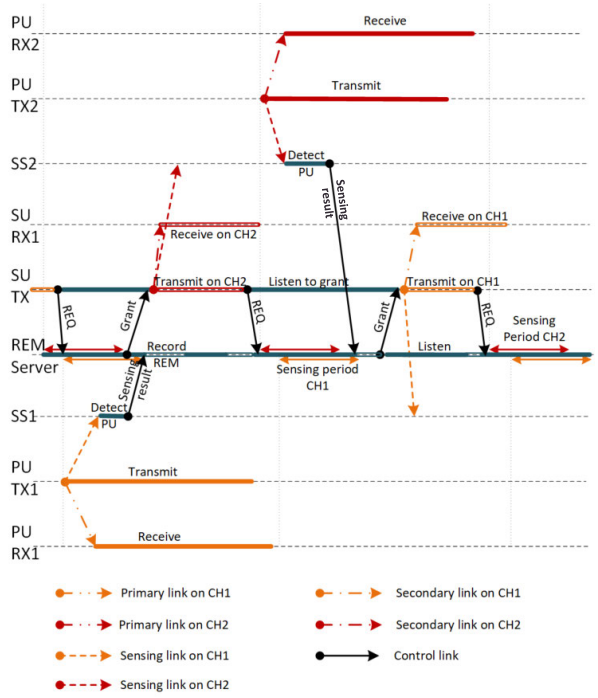

FIGURE 11. Proposed REM construction protocol.

TABLE 1. Notations used in DSA algorithm.

Notation	Description
d_{PU_CH1}	PU CH1 transmit duration
d_{PU_CH2}	PU CH2 transmit duration
Δt_{PU}	Waiting time for a sensor report to received by REM
SU_TX	SU transmitter
Δt_{SU}	Propagation delay from REM to SU_TX
d_{SU}	SU transmit duration
$t_{r\_PU\_CH1}$	PU CH1 last sensing report time
$t_{r\_PU\_CH2}$	PU CH2 last sensing report time
$t_{g\_SU\_CH1}$	SU CH1 last granted time
$t_{g\_SU\_CH2}$	SU CH2 last granted time
$t_{s\_PU\_CH1}$	PU CH1 current slot start time
$t_{e\_PU\_CH1}$	PU CH1 current slot end time
$t_{s\_PU\_CH2}$	PU CH2 current slot start time
$t_{e\_PU\_CH2}$	PU CH2 current slot end time
F_{CH1}	True if CH1 is available
F_{CH2}	True if CH2 is available
G_{SU}	SU grant status
I_g	Grant ID

PU activity in both CH1 and CH2. During the interval T_1, both channels remain occupied, and at t_2, CH1 becomes available after the sensing period, allowing SU transmission for a duration of d_{SU}. Similarly, at t_3, both channels are occupied, prompting the DSA algorithm to allocate CH2 to the SU at t_4 once it becomes free. SU TX transmits on CH2 for d_{SU} duration. If the SU requests transmission at t_5, DSA assigns CH1 and CH2 sequentially at t_6 and t_7 based on channel availability. At t_7, both channels are unoccupied for a duration of T_4, enabling the SU to transmit on CH1 and CH2.

Algorithm 3 Channel Availability Analysis for Channel i

Inputs: $t_{g\_SU\_CHi}$, $t_{r\_PU\_CHi}$, $t_{s\_PU\_CHi}$, $t_{e\_PU\_CHi}$
Output: Channel availability status F_{CHi}
Initialisation: $F_{CHi} \leftarrow False$
if $t_{g\_SU\_CHi}$ is not None AND $t - t_{g\_SU\_CHi} \leq d_{SU}$ **then**
    $F_{CHi} \leftarrow False$
else if $t_{r\_PU\_CHi} == t_{s\_PU\_CHi}$ **then**
    $F_{CHi} \leftarrow False$
else if $t_{s\_PU\_CHi} - t_{r\_PU\_CHi} \geq d_{PU\_CHi}$ **then** // There is no report for the next slot, channel could be free
    if $t - t_{s\_PU\_CHi} < \Delta t_{PU}$ **then** // Waiting for next report to arrive
        $F_{CHi} \leftarrow False$
    else
        if $t_{e\_PU\_CHi} - t > d_{SU} + \Delta t_{SU}$ **then** // Remaining time is sufficient for SU TX
            $F_{CHi} \leftarrow True$
        else // Time is not sufficient for SU TX
            $F_{CHi} \leftarrow False$
        end if
    end if
end if

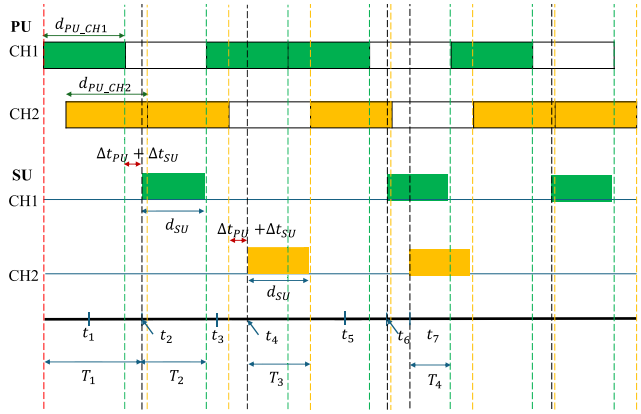

FIGURE 12. An example of random PU activity of CH1 & CH2 and SU dynamic spectrum access in cognitive network.

V. PERFORMANCE METRICS

To quantitatively evaluate the performance enhancement of the system, measurement reports are collected from both transmitters and receivers, as illustrated in Fig. 13. Spectral occupancy data is obtained from transmitters (PU TX, SU TX) through TX reports, while RX reports are gathered from all receivers (PU RX1, PU RX2, SU RX1 and SU RX2) to analyse throughput and overall system efficiency.

1) THROUGHPUT

Throughput T_p quantifies the effective data transmission rate in a communication system, measured in bits per second (bps). It is defined as the total number of successfully decoded

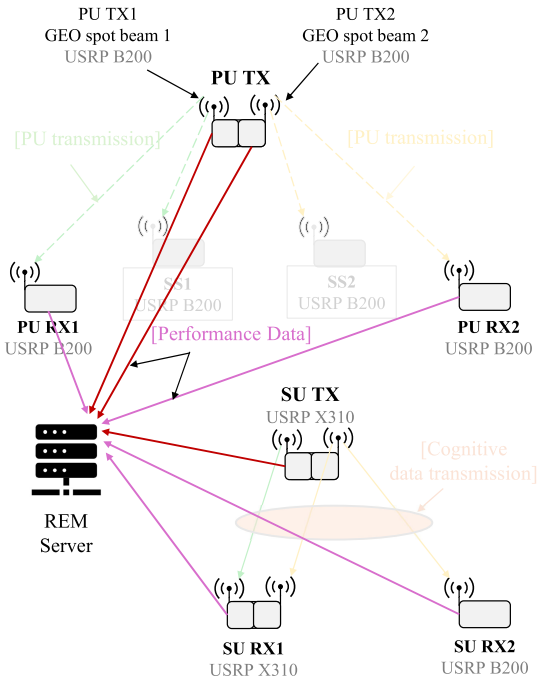

FIGURE 13. REM architecture for performance reporting links.

TABLE 2. Key system setup parameters.

Parameter	Description	Value
CH1	Frequency of CH1	5.727 GHz
CH2	Frequency of CH2	5.729 GHz
d_{PU_CH1}	PU CH1 transmit duration	1.14752 s
d_{PU_CH2}	PU CH2 transmit duration	1.14752 s
Δt_{PU}	Waiting time for a sensor report to received by REM	0.1 s
d_{SU}	SU transmit duration	0.28704 s
Γ	Sensing threshold	18
g_{PU}	PU TX transmission gain	60 dB
g_{SU}	SU TX transmission gain	10 dB
L_P	Preamble length	128
L	ZC sequence length	63

bits P_s at the receiver over a given observation period T_S.

$$T_p = \frac{P_s}{T_s} \tag{5}$$

2) SPECTRAL OCCUPANCY

Spectral occupancy S is calculated as the proportion of time a channel is actively used by PU, $S_{PU} = \frac{T_{PU}}{T_s}$, or SU, $S_{SU} = \frac{T_{SU}}{T_s}$, within a fixed observation period T_s.

$$S = S_{PU} + S_{SU} \tag{6}$$

3) MISSED DETECTIONS

In the sensing performance analysis of a cognitive system, missed detections refer to instances where the system fails to identify the presence of a real signal, event, or target. This type of error, also known as a false negative, occurs when an actual signal is classified as absent, leading to potential failures in decision-making. In a cognitive radio

Algorithm 4 REM Dynamic Spectrum Allocation

Initialisation:
Set last estimated PU transmission started times to None: $t_{r\_PU\_CH1} \leftarrow None$, $t_{r\_PU\_CH2} \leftarrow None$
Set SU granted time to None: $t_{g\_SU\_CH1} \leftarrow None$, $t_{g\_SU\_CH2} \leftarrow None$
Set current slot start and end times to None: $t_{s\_PU\_CH1} \leftarrow None$, $t_{e\_PU\_CH1} \leftarrow None$, $t_{s\_PU\_CH2} \leftarrow None$, $t_{e\_PU\_CH2} \leftarrow None$
Set PU_CH0 and PU_CH1 availability status to False: $F_{CH1} \leftarrow False$ and $F_{CH2} \leftarrow False$
Set status of SU channel grant: $G_{SU} \leftarrow False$
while NOT G_{SU} **do**
  $I_g \leftarrow$ findGrantId
  if I_g is -1 **then**
    Wait(Δt) // Wait and query again.
  else
    $G_{SU} \leftarrow True$
    Output: I_g
  end if
end while
function findGrantId // This function returns channel grant ID
  Query last TX reports of CH1 and CH2 from database table
  Update $t_{r\_PU\_CH1}$ and calculate $t_{s\_PU\_CH1}$ using (4a) and $t_{e\_PU\_CH1}$ using (4b)
  Update $t_{r\_PU\_CH2}$ and calculate $t_{s\_PU\_CH1}$ using (4a) and $t_{e\_PU\_CH1}$ using (4b)
  // Update F_{CH1} and F_{CH2} based on sensor reports
  $F_{CH1} \leftarrow$ channelStatus($t_{g\_SU\_CH1}$, $t_{r\_PU\_CH1}$, $t_{s\_PU\_CH1}$, $t_{e\_PU\_CH1}$)
  $F_{CH2} \leftarrow$ channelStatus($t_{g\_SU\_CH2}$, $t_{r\_PU\_CH2}$, $t_{s\_PU\_CH2}$, $t_{e\_PU\_CH2}$)
  if F_{CH1} AND F_{CH2} **then**
    $I_g = 2$ // Both channels are available
  else if F_{CH1} **then**
    $I_g = 0$ // Only CH1 is available
  else if F_{CH2} **then**
    $I_g = 1$ // Only CH2 is available
  else
    $I_g = -1$ // Both channels are occupied
  end if
  return I_g
end function
function channelStatus($t_{g\_SU\_CHi}$, $t_{r\_PU\_CHi}$, $t_{s\_PU\_CHi}$, $t_{e\_PU\_CHi}$)
  $F_{CHi} \leftarrow$ Find channel's status based on Algorithm 3
  return F_{CHi}
end function

network, if a sensor fails to detect an active primary user in a frequency band, it may cause interference, degrading the overall network performance.

VI. MEASUREMENT RESULTS AND DISCUSSION

The development platform operates in the 5 GHz band, selected for its regulatory flexibility and ease of implementation. Although designed for unlicensed bands, the cognitive radio concepts apply to licensed satellite frequencies in practical deployments. The ISM band presents limited available bandwidth and is subject to interference from coexisting devices, reducing the number of interference-free channels for reliable communication. Furthermore, wideband signal processing on SDRs introduces additional latency due to the computational demands of digital signal processing, impacting real-time performance. To balance bandwidth utilisation and processing constraints, a channel bandwidth of 400 kHz is selected. Specifically, channels CH1 and CH2 operate at centre frequencies of 5.727 GHz and 5.729 GHz, respectively, each occupying 400 kHz. During preamble generation, the PU and SU transmitters are assigned root indices $q_{p,1} = 25$, $q_{p,2} = 29$ and $q_{s,1} = 31$ and $q_{s,2} = 37$, respectively. The preamble is constructed by pre-padding $L_{pre} = 32$ zeros, followed by the ZC sequence, and post-padding $L_{post} = 33$ zeros. We consider PU transmission durations $d_{PU\_CH1} = 1.14752$ s and SU transmission duration $d_{SU} = 0.28704$ s. In practical scenarios, slot durations must account for the propagation delay associated with LEO motion. The key system parameters utilised for system development are summarised in Table 2.

The visualisation platform integrates sensing reports, IQ sensing data, spectral occupancy analysis, and throughput evaluation. System performance is assessed under three scenarios:

- The PU transmits randomly on CH2 while maintaining continuous transmission on CH1.
- The PU transmits randomly on CH1 while maintaining continuous transmission on CH2.
- The PU transmits randomly across both CH1 and CH2.

In Fig.14, sensing reports from secondary sensors SS1 and SS2 are utilised to infer PU activity over time across two channels, CH1 and CH2. In this figure, the y-axis denotes time in the HH:mm:ss format, while the x-axis corresponds to the PU channel IDs (CH1 and CH2). The spectrogram is derived from IQ data collected via the SIQ node, visualises signal power over the 5724 MHz to 5728 MHz frequency band. The y-axis represents time in HH:mm:ss format, while the x-axis corresponds to frequency in MHz. Signal intensity is colour-coded, with red indicating high-power transmissions and blue indicating low-power levels. Extended-duration transmissions are indicative of PU activity, whereas short-duration high-power bursts correspond to SU transmissions. A persistent red line at 5724 MHz represents the DC component, as this frequency serves as the centre of the observed band. In the subsequent performance evaluation, we present spectrum occupancy metrics for CH1 and CH2, derived from the estimated PU and SU activity as outlined in section V-2. Additionally, throughput analysis for the receiving nodes is provided in section V-1, including primary user receivers (PU RX1 and PU RX2) and secondary user receivers (SU RX1 and SU RX2).

In Fig. 14a, PU continuously transmits on CH1, while CH2 follows a random pattern. SU RX1 and SU RX2 share CH2 under equal access conditions, with the scheduler assigning CH1 for their transmissions. CH1 maintains 100% occupancy, while CH2 fluctuates around 50%, increasing to 60% with SU transmissions. PU RX1 achieves the highest throughput due to uninterrupted PU transmission, while PU RX2 experiences lower throughput due to CH2's randomness. SU RX1 and SU RX2 attain similar throughput by alternately accessing CH2.

In Fig. 14b, PU transmits randomly on CH1 and continuously on CH2. SU RX1 has exclusive CH1 access, while SU RX2, restricted to CH2, receives no data. CH2 remains fully occupied, while CH1 averages 50% occupancy, increasing with SU activity. PU RX2 achieves the highest throughput, PU RX1 experiences lower rates due to CH1's intermittency, and SU RX1 benefits from exclusive CH1 access, while SU RX2 experiences zero throughput.

Fig. 14c represents the scenario in which PU TX on both CH1 and CH2 follows random transmission patterns. The SU TX scheduler dynamically allocates CH1 and CH2 based on their availability for SU RX1 and SU RX2. In the spectral occupancy analysis, as expected, both CH1 and CH2 exhibit increased occupancy due to SU TX transmissions, demonstrating the adaptive nature of the cognitive system. Regarding throughput, PU RX1 and PU RX2 achieve comparable data rates, influenced by the stochastic transmission patterns and the successful decoding of received data. As anticipated, SU RX1 attains higher throughput than SU RX2, as it has access to both CH1 and CH2, whereas SU RX2 is limited to a single channel. In summary, across all scenarios, spectral occupancy and system throughput improve due to the cognitive system's dynamic spectrum access capabilities. Furthermore, the transmission reports closely align with the IQ sensing data, validating the accuracy of the sensing mechanism.

We evaluate the performance of the proposed cognitive system under varying PU TX transmission gain levels, as illustrated in Fig. 15, across three scenarios:

- Scenario S1: PU TX channels CH1 and CH2 exhibit random transmission patterns.
- Scenario S2: PU TX channels CH1 and CH2 exhibit an alternative transmission pattern, where each channel cyclically alternates between active and idle states in consecutive time slots.
- Scenario S3: PU TX CH1 operates continuously, while PU TX CH2 follows an alternative transmission pattern.

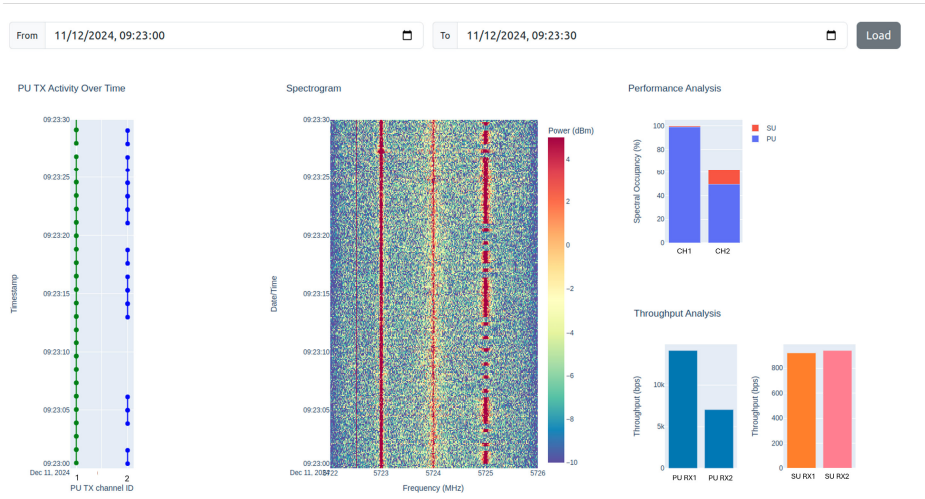

(a) PU employs a random transmission pattern on CH2 while ensuring continuous data transmission on CH1.

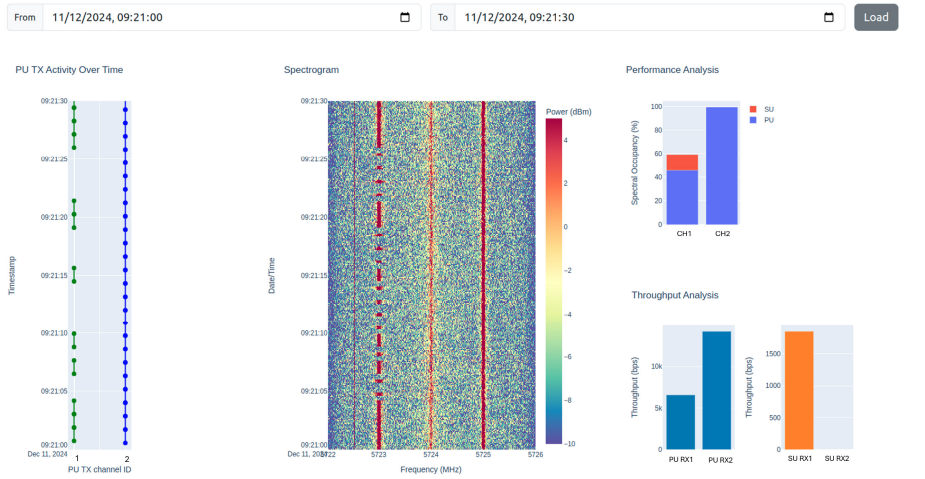

(b) PU employs a random transmission pattern on CH1 while ensuring continuous data transmission on CH2.

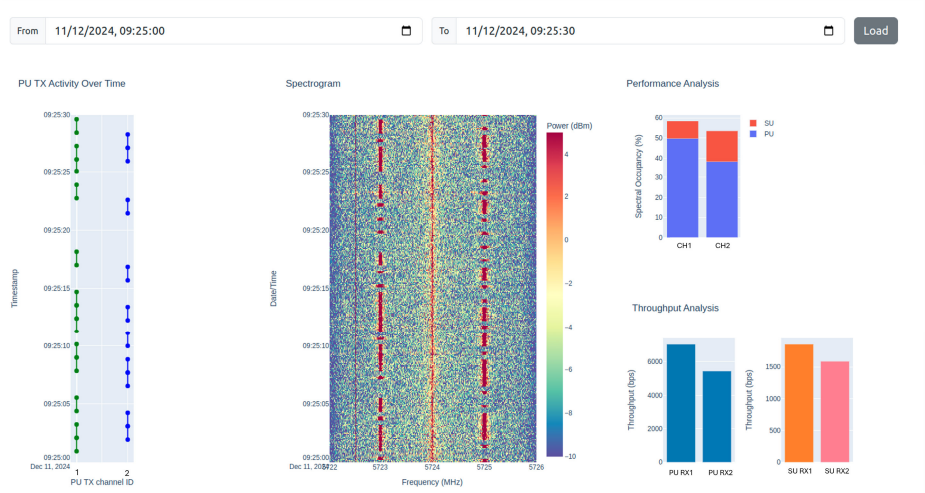

(c) PU transmits data with a random transmission pattern over CH1 and CH2.

FIGURE 14. **Cognitive satellite network: both primary user and secondary user share the spectrum.**

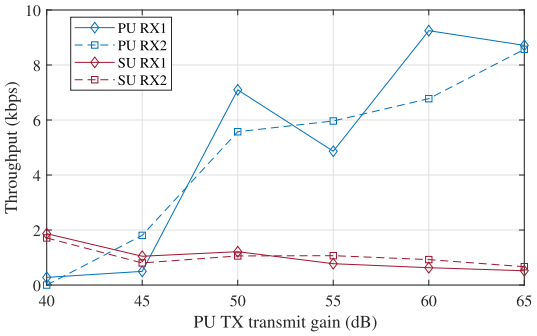

(a) Throughput analysis: Scenario S1.

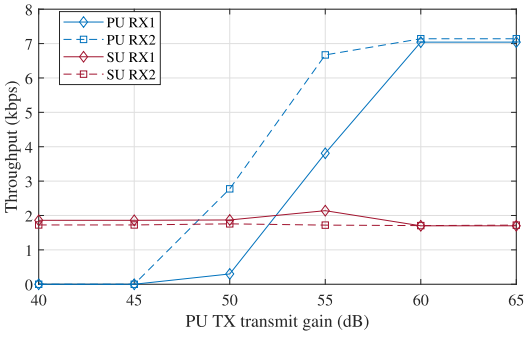

(b) Throughput analysis: Scenario S2.

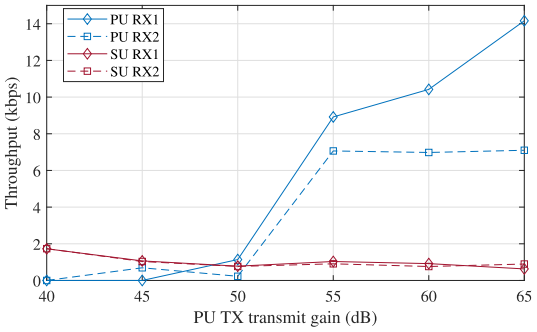

(c) Throughput analysis: Scenario S3.

FIGURE 15. Throughput analysis of the proposed cognitive system analysis under three scenarios: S1, S2, and S3.

Given the random transmission behaviour of both CH1 and CH2 in S1, spectral occupancy fluctuates accordingly. Throughput is also influenced by PU TX transmission gain, as shown in Fig. 15a. Specifically, for PU receivers (PU RX1 and PU RX2), throughput increases with PU TX transmission gain. However, at lower transmission gain levels, particularly at 40 dB and 45 dB, throughput is significantly reduced due to a low signal-to-noise ratio (SNR), which impairs the accurate decoding of received data. Conversely, SU receivers (SU RX1 and SU RX2) experience an increase in throughput under low PU TX transmission gain conditions. This occurs because reduced PU transmission gain leads to a degradation in sensor detection performance, resulting in an increased rate of missed detections and, consequently, an increase in unnecessary SU transmissions. As depicted in Fig. 15b, PU receiver throughput follows a similar trend in S2, rising

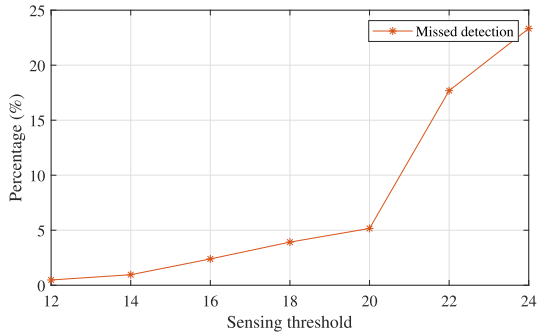

FIGURE 16. Analysis of the performance of the proposed sensing algorithm using missed detections.

with PU TX gain but deteriorating at low levels due to SNR reduction. However, SU receiver throughput remains stable across conditions. Compared to random PU transmission, the alternative pattern reduces PU channel throughput but enhances SU access opportunities, improving SU receiver performance.

In S3, CH1 remains fully occupied due to continuous PU TX1 transmission. PU receiver follows the same behaviour, throughput declines at low PU TX gain due to increased decoding errors from reduced SNR. SU receivers share CH2 equally, maintaining similar throughput. However, if CH2 reaches full occupancy. due to continuous PU TX2 transmission, SU RX2 loses all transmission opportunities, reducing its throughput to zero.

The performance of the proposed sensing algorithm in Algorithm 1 depends on the sensing threshold. We analysed the performance of the proposed sensing algorithm in terms of missed detections against the threshold as depicted in Fig. 16. We keep all parameters constant except the sensing threshold during this analysis. We can observe that the number of missed detections increases with the higher threshold value, meaning there will be more SU transmissions causing interference to the PU transmission, degrading overall system performance.

To further validate system functionality, we introduce controlled interference to assess the performance of the proposed platform. Specifically, we incorporate a dedicated interference node, hereafter referred to as the interferer, configured to generate Gaussian noise that impacts both communication channels CH1 and CH2. The interferer is positioned near the PU RX2 and SS2 to evaluate the asymmetrical effects of interference on sensing and receiving nodes. The PU TX operates with a fixed transmit gain of 60 dB, and an alternative transmission pattern is employed to simulate dynamic traffic conditions. We analyse the missed detection performance of sensing nodes SS1 and SS2 across a range of interferer transmit gains, spanning 40 dB to 70 dB, as shown in Fig. 17. The results reveal a significant increase in missed detection rates beyond 55 dB, leading to erroneous spectrum access grants for the SU TX and resulting in unintended interference to PU communications. Due to

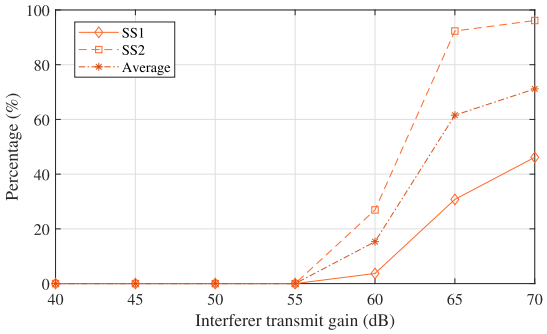

FIGURE 17. Missed detection performance of the proposed sensing algorithm under varying interference levels, with fixed PU TX gain and transmission pattern.

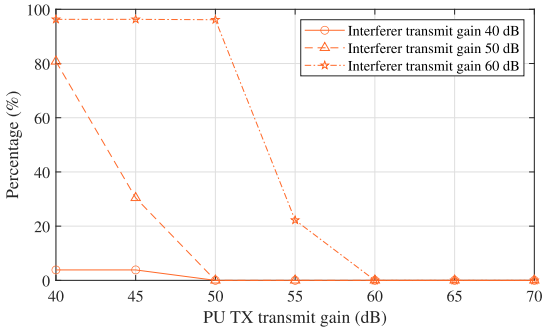

FIGURE 18. Missed detection performance of the proposed sensing algorithm under varying interference levels, obtained by jointly varying PU transmit power and interferer transmit power.

the interferer's proximity to SS2, its sensing performance deteriorates more rapidly with increasing interference power. Overall, the system demonstrates acceptable missed detection performance for signal-to-interference ratios (SIR) exceeding 0 dB.

Next, we focus solely on the performance of sensing node SS2. We evaluate missed detection behaviour under varying primary user transmit power and interference levels, as illustrated in Fig. 18. Specifically, the PU TX transmit gain is varied from 40 dB to 70 dB, while the interferer transmit gain is fixed at 40 dB, 50 dB, and 60 dB in separate test cases. The results indicate that when the interferer transmit gain is 40 dB, its effect on SS2's sensing performance is negligible, resulting in a consistently low missed detection rate. However, as the interferer transmit gain increases, a corresponding degradation in detection accuracy is observed. Notably, when the SIR reaches 0 dB, the missed detection rate approaches zero, indicating robust sensing performance under balanced signal and interference conditions.

Finally, we evaluate the throughput performance of each receiver node, as shown in Fig. 19. The results indicate that the PU throughput remains relatively stable up to an interference power of 55 dB, beyond which it begins to decline due to increased interference. Furthermore, the throughput of PU RX2 experiences a significant decline

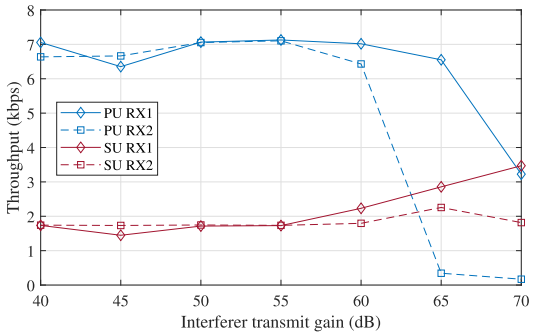

FIGURE 19. Throughput analysis for different interference levels.

as interference power increases. This is due to its physical proximity to the interferer, which leads to severe degradation in decoding performance under high interference conditions. The SU RX throughput exhibits a noticeable increase beyond the 55 dB threshold. This is attributed to the degradation in sensing node performance, as previously observed in Fig. 17, which leads to a higher rate of missed detections. As a result, secondary user transmissions are granted more frequently, including in instances where the spectrum is occupied by the PU, introducing harmful interference and compromising overall cognitive network performance.

VII. FUTURE WORK

As this work focuses on a proof-of-concept, laboratory-scale demonstration platform using SDRs, the primary objective is to establish a flexible and reconfigurable environment for cognitive GEO-LEO satellite network experimentation. Future work will focus on extending this platform toward a more realistic and comprehensive testbed capable of emulating the complex conditions of real-world satellite networks. The existing setup simplifies several real-world factors due to laboratory constraints, and future enhancements are needed to bridge this gap. Specifically, operation within the ISM bands limits available bandwidth and is prone to interference, reducing the number of clean, interference-free channels for reliable communication. Moreover, wideband signal processing on SDR platforms introduces non-negligible latency due to the computational complexity of digital baseband processing, posing challenges for real-time system performance. Nonetheless, the proposed system remains scalable to wideband operation, as SDR platforms inherently support wideband signal processing capabilities. The current system experiences occasional packet losses and CRC failures. Latency measurements indicate that delays are primarily introduced by buffering within the SDR processing chain, with negligible contributions from network-induced delay. Future work will involve detailed profiling of these latency components and packet loss mechanisms to further optimise system performance. Furthermore, the platform does not presently account for satellite mobility, Doppler effects, or other orbital dynamics. Incorporating real-time

orbital modelling and time-varying channel emulation will be an essential and technically challenging direction for future development to better capture the behaviour of GEO-LEO satellite communications.

VIII. CONCLUSION

In conclusion, cognitive radio technology plays a vital role in advancing modern telecommunications by enabling intelligent, adaptive communication systems. This study demonstrates the implementation of a cognitive GEO-LEO dual satellite system using software-defined radios, where the GEO satellite serves as the primary user and the LEO satellite as the secondary user. We employed two types of SDRs: USRPB200s and USRPX310s. Through the development of a preamble detection-based sensing algorithm, a REM server for control plane data management, and a dynamic spectrum access algorithm, we successfully enable cognitive behaviour in satellite networks. The evaluation of spectral occupancy, throughput, and missed detections highlights the effectiveness of our approach in enhancing spectral efficiency, resource utilisation, and overall network performance. These findings contribute to the development of more scalable, resilient, and cost-effective satellite communication systems.

REFERENCES

[1] Q. T. Ngo, Z. Tang, B. Jayawickrama, Y. He, E. Dutkiewicz, and B. Senanayake, "Timeliness of information in 5G nonterrestrial networks: A survey," *IEEE Internet Things J.*, vol. 11, no. 21, pp. 34652–34675, Nov. 2024.

[2] W. S. H. M. W. Ahmad, N. A. M. Radzi, F. S. Samidi, A. Ismail, F. Abdullah, M. Z. Jamaludin, and M. N. Zakaria, "5G technology: Towards dynamic spectrum sharing using cognitive radio networks," *IEEE Access*, vol. 8, pp. 14460–14488, 2020.

[3] S. Basnet, Y. He, E. Dutkiewicz, and B. A. Jayawickrama, "Resource allocation in moving and fixed general authorized access users in spectrum access system," *IEEE Access*, vol. 7, pp. 107863–107873, 2019.

[4] Q. Wu, J. Xu, Y. Zeng, D. W. K. Ng, N. Al-Dhahir, R. Schober, and A. L. Swindlehurst, "A comprehensive overview on 5G-and-Beyond networks with UAVs: From communications to sensing and intelligence," *IEEE J. Sel. Areas Commun.*, vol. 39, no. 10, pp. 2912–2945, Oct. 2021.

[5] C. Wang, D. Bian, S. Shi, J. Xu, and G. Zhang, "A novel cognitive satellite network with GEO and LEO broadband systems in the downlink case," *IEEE Access*, vol. 6, pp. 25987–26000, 2018.

[6] Q. Tu Ngo, B. Jayawickrama, Y. He, and E. Dutkiewicz, "A novel satellite-based REM construction in cognitive GEO-LEO satellite IoT networks," *IEEE Internet Things J.*, vol. 12, no. 6, pp. 7532–7548, Aug. 2024.

[7] Y.-C. Liang, J. Tan, H. Jia, J. Zhang, and L. Zhao, "Realizing intelligent spectrum management for integrated satellite and terrestrial networks," *J. Commun. Inf. Netw.*, vol. 6, no. 1, pp. 32–43, Mar. 2021.

[8] Q. T. Ngo, B. A. Jayawickrama, Y. He, E. Dutkiewicz, K. Weththasinghe, N. Clark, E. Arbon, and M. Bowyer, "Optimizing spectrum sensing in cognitive GEO-LEO satellite networks: Overcoming challenges for effective spectrum utilization," *IEEE Veh. Technol. Mag.*, early access, Feb. 5, 2025.

[9] P. Gu, R. Li, C. Hua, and R. Tafazolli, "Dynamic cooperative spectrum sharing in a multi-beam LEO-GEO co-existing satellite system," *IEEE Trans. Wireless Commun.*, vol. 21, no. 2, pp. 1170–1182, Feb. 2022.

[10] K. Weththasinghe, N. Clark, Q. T. Ngo, B. Jayawickrama, Y. He, E. Dutkiewicz, and R. P. Liu, "L-band spectral opportunities for cognitive GEO-LEO dual satellite networks," in *Proc. 22nd Int. Symp. Commun. Inf. Technol. (ISCIT)*, Oct. 2023, pp. 48–51.

[11] C. Zhang, C. Jiang, J. Jin, S. Wu, L. Kuang, and S. Guo, "Spectrum sensing and recognition in satellite systems," *IEEE Trans. Veh. Technol.*, vol. 68, no. 3, pp. 2502–2516, Mar. 2019.

[12] Q. T. Ngo, B. A. Jayawickrama, Y. He, and E. Dutkiewicz, "Multi-agent DRL-based RIS-assisted spectrum sensing in cognitive satellite-terrestrial networks," *IEEE Wireless Commun. Lett.*, vol. 12, no. 12, pp. 2213–2217, Dec. 2023.

[13] J. Hu, G. Li, D. Bian, S. Shi, R. Ge, and L. Gou, "Energy-efficient cooperative spectrum sensing in cognitive satellite terrestrial networks," *IEEE Access*, vol. 8, pp. 161396–161405, 2020.

[14] R. G. Mattingly and J. G. Metcalf, "Fast adaptive spectrum sensing using hardware optimized, cell averaging estimation for cognitive radio and radar applications," *IEEE Trans. Aerosp. Electron. Syst.*, vol. 59, no. 5, pp. 5084–5096, May 2023.

[15] E. Dutkiewicz, Y. He, B. A. Jayawickrama, and H. V. Abeywickrama, "Radio environment maps generation and spectrum sensing testbed for spectrum sharing in 5G networks," in *Proc. IEEE-APS Topical Conf. Antennas Propag. Wireless Commun. (APWC)*, Sep. 2017, pp. 33–36.

[16] J. Manco, I. Dayoub, A. Nafkha, M. Alibakhshikenari, and H. B. Thameur, "Spectrum sensing using software defined radio for cognitive radio networks: A survey," *IEEE Access*, vol. 10, pp. 131887–131908, 2022.

[17] C. Politis, S. Maleki, J. M. Duncan, J. Krivochiza, S. Chatzinotas, and B. Ottesten, "SDR implementation of a testbed for real-time interference detection with signal cancellation," *IEEE Access*, vol. 6, pp. 20807–20821, 2018.

[18] M. V. Lipski, S. Kompella, and R. M. Narayanan, "Practical implementation of adaptive threshold energy detection using software defined radio," *IEEE Trans. Aerosp. Electron. Syst.*, vol. 57, no. 2, pp. 1227–1241, Apr. 2021.

[19] I. Dey, P. S. Rossi, M. M. Butt, and N. Marchetti, "Experimental analysis of wideband spectrum sensing networks using massive MIMO testbed," *IEEE Trans. Commun.*, vol. 68, no. 9, pp. 5390–5405, Sep. 2020.

[20] D. Capriglione, G. Cerro, L. Ferrigno, and G. Miele, "Effects of real instrument on performance of an energy detection-based spectrum sensing method," *IEEE Trans. Instrum. Meas.*, vol. 68, no. 5, pp. 1302–1312, May 2019.

[21] K. Weththasinghe, Q. T. Ngo, Y. He, B. Jayawickrama, and E. Dutkiewicz, "Cognitive GEO-LEO dual satellite networks: Multibeam sensing," in *Proc. 23rd Int. Symp. Commun. Inf. Technol. (ISCIT)*, Sep. 2024, pp. 105–109.

[22] 3GPP, *Physical Channels and Modulation (Release 8)*, document TS 36.211, Mar. 2009.

[23] 3GPP, *Nonsynchronized Random Access Structure for E-UTRA*, document R1-062630, Oct. 2006.

[24] M. Mueck, Y. He, B. Jayawickrama, and E. Dutkiewicz, "Methods and devices for user detection in spectrum sharing," U.S. Patent 10 681 558 B2, Jun. 20, 2024.

KITHMINI WETHTHASINGHE (Graduate Student Member, IEEE) received the B.Sc. (Hons.) degree in electronic and telecommunication engineering and the M.Sc. degree in telecommunications from the University of Moratuwa, Sri Lanka, in 2016 and 2022, respectively. She is currently pursuing the Ph.D. degree with the School of Electrical and Data Engineering, University of Technology Sydney, Sydney, NSW, Australia.

Her research interests include machine learning in wireless communications, satellite communications, and cognitive radio.

YING HE (Senior Member, IEEE) received the B.Eng. degree in telecommunications engineering from Beijing University of Posts and Telecommunications, Beijing, China, in 2009, and the Ph.D. degree in telecommunications engineering from the University of Technology Sydney, Sydney, NSW, Australia, in 2017.

She is currently a Senior Lecturer with the School of Electrical and Data Engineering, University of Technology Sydney. Her research interests include physical layer algorithms in wireless communication with machine learning, vehicular communications, spectrum sharing, and satellite communications.

QUYNH TU NGO (Senior Member, IEEE) received the B.Sc. degree (magna cum laude) in electrical engineering from California State University, Los Angeles, CA, USA, in 2013, the M.Sc. degree in telecommunications from Vietnam National University-University of Sciences, Ho Chi Minh City, Vietnam, in 2016, and the Ph.D. degree in computer science from La Trobe University, VIC, Australia, in 2023.

She is currently a Postdoctoral Research Fellow with the School of Electrical and Data Engineering, University of Technology Sydney, Australia. Her research interests include satellite communications, the IoT networks, intelligent non-terrestrial networks, and machine learning in wireless communications and networking.

BEESHANGA JAYAWICKRAMA (Senior Member, IEEE) received the B.E. degree (Hons.) in telecommunications engineering and the Ph.D. degree in electronic engineering from Macquarie University, Macquarie Park, NSW, Australia, in 2011 and 2015, respectively.

He is currently a Visiting Fellow with the University of Technology Sydney, Australia. He was extensively involved in spectrum sensing and interference mitigation research for spectrum access systems. His research interests include non-terrestrial networks, 5G/6G, cognitive radio, and signal processing.

ERYK DUTKIEWICZ (Senior Member, IEEE) received the B.E. degree in electrical and electronic engineering and the M.Sc. degree in applied mathematics from The University of Adelaide, Australia, in 1988 and 1992, respectively, and the Ph.D. degree in telecommunications from the University of Wollongong, Australia, in 1996. His industry experience includes management of the Wireless Research Laboratory, Motorola, in the early 2000s. He is currently the Associate Dean International of the Faculty of Engineering and IT, University of Technology Sydney, Australia. He also holds a professorial appointment with Hokkaido University, Japan. His current research interests include 5G/6G and the IoT networks.